Fast and robust quantum state transfer assisted by zero-energy interface states in a splicing Su-Schrieffer-Heeger chain

Lijun Huang [1,2] Zhi Tan [1,2] Honghua Zhong,[1,2,*] and Bo Zhu[2,†]

[1]*School of Life Science and Technology, Central South University of Forestry and Technology, Changsha 410004, China*

[2]*Institute of Mathematics and Physics, Central South University of Forestry and Technology, Changsha 410004, China*

(Received 13 March 2022; accepted 5 August 2022; published 19 August 2022)

We propose a fast, robust, and long-distance quantum state transfer (QST) protocol via a splicing Su-Schrieffer-Heeger (SSH) chain, where the interchain couplings vary with the change in the phase parameter and the single or splicing SSH chain can be designed by adjusting it. It is found that the existence of a zero-energy interface state (IFS) not only can improve the speed of QST but also can realize long-distance QST. Furthermore, we give the phase diagram in the parameter space of the transfer time T and the system's size N, where the different regions that can successfully implement QST via a single- or splicing-SSH-chain protocol are given. Therefore, we can choose the optimal QST protocol by adjusting only the phase parameter for different transfer times and system sizes. By numerically investigating the resilience of each protocol to static disorder, we reveal that the splicing-SSH-chain protocol is quite robust to both diagonal and off-diagonal disorders and clearly outperforms the single-SSH-chain protocol. By considering the environmental influence, rendering the Hamiltonian non-Hermitian by allowing energy to radiate away, our work shows that the QST protocol assisted by zero-energy IFS is more robust than previously expected and also outperforms the single-SSH-chain protocol.

DOI: 10.1103/PhysRevA.106.022419

I. INTRODUCTION

The basic task of quantum information processing is constructing a quantum network where states can be transferred in a coherent manner between two nodes [1–3]. In recent years, great effort has been made to obtain the optimal protocol for state transfer in a one-dimensional spin-$\frac{1}{2}$ chain that provides a simple and effective platform to implement quantum state transfer (QST), which can be realized in a variety of physical systems, including coupled waveguides [4–6], acoustic cavities [7], diamond vacancies [8], superconducting circuits [9,10], arrays of quantum dots [11], driven optical lattices [12], NMR [13], and nanoelectromechanical networks [14]. However, due to the inevitable decoherence of quantum state and device imperfections, the degree a quantum state can be transferred with good fidelity will be limited [15,16], which induces a trade-off between the transfer speed, distance, and robustness, as increasing one results in a decrease of the others and vice versa. The quantum speed limit for transferring a state along a spin chain has been studied for various protocols [17–23], and the role of different sources of decoherence in QST protocols and ways to circumvent their impact have been discussed [24–33], including optimal control by applying an external parabolic magnetic field [19] and a shortcut to adiabaticity [32,33].

A very promising platform for the realization of an efficient QST protocol comes from the Su-Schrieffer-Heeger (SSH) chain [1,10,34–42], whose most appealing property is that they host a zero-energy edge mode which is robust to different sources of quantum decoherence due to their topological protection. Usually, this QST protocol relies on the time evolution of a specially designed Hamiltonian and requires very precise control of a tunable coupling parameter such as robust QST via tunable coupling between adjacent sites [10], fast and robust QST by next-nearest-neighbor couplings [43], high-fidelity and long-distance entangled-state transfer via periodically driven coupling [3], and fast and robust QST via exponential time-driving coupling [44]. However, these previous studies have been limited to considering a homogeneous SSH chain. This is a rather challenging task in experiment, as the adiabatic change in the coupling strength must be tuned uniformly. Therefore, the protocol of a splicing SSH chain may be more easily operated in experiment; in this protocol two types of localized states can appear according to the interface position: one is the edge state that appears at the interface between the chain and vacuum, and the other is the interface state that appears at the interface between different chains. Especially, research on the role of the interface state in the process of QST in such a splicing SSH chain is still lacking.

In this work, we propose a fast and robust QST protocol via a splicing-SSH-chain, where the interchain couplings vary with the change in phase parameter and the single- or splicing-SSH-chain can be designed by adjusting it. Two types of zero-energy interface states (IFSs) are presented; the first one is an even function for the interfaces at odd sites, and the second one is an odd function for the interfaces at even sites. It is found that the existence of zero-energy IFSs not only can improve the speed of QST but also can realize long-distance QST compared to the single-SSH-chain protocol. Furthermore,

*hhzhong115@163.com

†zhubo163ky@163.com

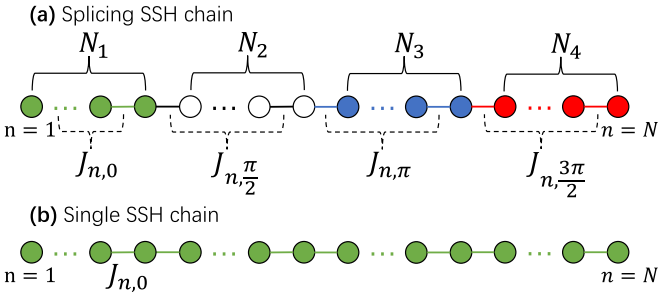

FIG. 1. Schematic diagram of different SSH chains. (a) Splicing SSH chain, where the coupling strengths of the four subchains are set as $J_n = J_{n,0}$ for $n \in [1, N_1 - 1]$, $J_n = J_{n,\frac{\pi}{2}}$ for $n \in [N_1, N_1 + N_2 - 1]$, $J_n = J_{n,\pi}$ for $n \in [N_1 + N_2, N - N_4 - 1]$, and $J_n = J_{n,\frac{3\pi}{2}}$ for $n \in [N - N_4, N - 1]$. (b) Single SSH chain, where the coupling strength equably is set as $J_n = J_{n,0}$ for $n \in [1, N - 1]$.

we give the phase diagram in the parameter space of the transfer time T and the system size N. The different regions that can successfully implement QST are revealed via the single- or splicing-SSH-chain protocol. Therefore, we can choose the optimal QST protocol by adjusting only the phase parameter in the coupling. By numerically investigating the resilience of each protocol to static disorder, we reveal that the splicing-SSH-chain protocol is quite robust to both diagonal and off-diagonal disorders and obviously outperforms the single-SSH-chain protocol. We further consider the environmental influence by rendering the Hamiltonian non-Hermitian by allowing energy to radiate away, and it is shown that the QST protocol assisted by zero-energy IFSs is more robust than previously expected and also outperforms the single-SSH-chain protocol. Our proposal may provide an experimentally friendly way to achieve QST.

The rest of this article is organized as follows. In Sec. II, we present QST protocols assisted by zero-energy IFSs. We introduce the Hamiltonian of the system together with the corresponding protocols in Sec. II A and then discuss the energy spectrum, zero-energy states, speed of the transfer, and phase diagram in Secs. II B and II C. In Sec. III, we analyze the impact of on- and off-diagonal disorder. In Sec. IV, we study the effect of the environment on the behavior of each protocol. Finally, we give a conclusion in Sec. V.

II. QST PROTOCOLS ASSISTED BY ZERO-ENERGY INTERFACE STATES

A. Model

We start by considering a splicing SSH chain describing a spin-$\frac{1}{2}$ chain acting as a data bus for transferring a quantum state. The Hamiltonian describes N spins, $N = \sum_{i=1}^{4} N_i$, which are spliced by four conventional SSH models with site numbers N_1, N_2, N_3, and N_4 [see Fig. 1(a)]. To realize QST via a topology protected zero-energy IFS, here, we consider N to be an odd number and $N_i - N_j = 0$ or ± 1. When we restrict ourselves to the one-excitation subspace, that is, all spins point down but one, the Hamiltonian can be written as

$$\mathcal{H} = \sum_{n=1}^{N-1} J_n(|n\rangle\langle n+1| + \text{H.c.}) + \sum_{n=1}^{N} B_n|n\rangle\langle n|, \tag{1}$$

with

$$J_n = \begin{cases} J_{n,0} & \text{for } n \in [1, N_1 - 1], \\ J_{n,\frac{\pi}{2}} & \text{for } n \in [N_1, N_1 + N_2 - 1], \\ J_{n,\pi} & \text{for } n \in [N_1 + N_2, N - N_4 - 1], \\ J_{n,\frac{3\pi}{2}} & \text{for } n \in [N - N_4, N - 1]. \end{cases} \tag{2}$$

Here, $J_{n,\varphi} = g_0 + g_1 \cos(n\pi + \theta - \varphi)$ is the nearest-neighbor coupling strength between the nth and $(n+1)$th sites, where φ and θ respectively represent the initial phase and adiabatic parameters. It is worth noting that, because the coupling strength can periodically change $J_{n,\varphi} = J_{n,\varphi+2\pi}$, our system can be spliced by arbitrary numbers of SSH models by setting different coupling strengths $J_{n,\varphi}$ (see the Appendix). The basis $|n\rangle$ denotes that the nth site of the chain is excited, corresponding to the Fock state $|0_1 0_2 \cdots 1_n \cdots 0_N\rangle$. B_n denotes a local magnetic field applied at each site. Because an arbitrary value of the magnetic field corresponds to a global shift on the energy spectrum, without loss of generality, we choose $B_n = 0$ in our work. Our system also can be reduced to a single SSH chain by setting coupling strength $J_n = J_{n,0}$ for $n \in [1, N - 1]$ [see Fig. 1(b)]. The aim of the protocol we consider is to transfer a single site excitation from the first site $|1\rangle$ to the last site $|N\rangle$ of the chain by adiabatically controlling the parameters θ during the dynamical evolution. The quantity that determines how faithfully the transfer has occurred is the fidelity, which in our case can be defined as

$$F = |\langle N|\psi(T)\rangle|^2, \tag{3}$$

where $|\psi(T)\rangle$ denotes the final state, obtained by numerically solving the time-dependent Schrödinger equation for $\mathcal{H}$, and T corresponds to the transfer time of the quantum state.

In the case of a single SSH chain, the zero-energy edge states protected by topology can be exploited as a topologically protected quantum channel to realize the QST [10,44]; the main reason is that the positions of the zero-energy edge state are exchanged due to the change in the coupling strength. However, the realization of uniformly adjusting the coupling strength for a long SSH chain still remains a challenge in experiment. Therefore, the splicing SSH chain is an even more practical system, which may be able to induce diverse zero-energy states, including a zero-energy edge state (EGS), zero-energy extended state (ETS), and zero-energy IFS. As we will show, the zero-energy IFS can assist in long-distance QST.

B. Energy spectrum and zero-energy states

To show QST assisted by the zero-energy IFSs, we consider the energy spectrum and corresponding zero-energy states under different coupling strengths by adjusting the parameter θ. A typical example is displayed in Fig. 2 by choosing total lattice sites $N = 41$, $g_0 = g_1 = 1$, and $(N_1, N_2, N_3, N_4) = (10, 10, 10, 11)$. An inspection of the energy diagram shows that the zero-energy states always exist and are threefold degenerate for some fixed parameters θ. As the parameter θ changes, three different zero-energy states can transform each other, and the zero-energy state is nondegenerate in the parameter space $0.7\pi \leqslant \theta \leqslant 1.8\pi$ [see Figs. 2(a) and 2(b)]. For the sake of clarity, we give the corresponding zero-energy eigenstates for the parameters

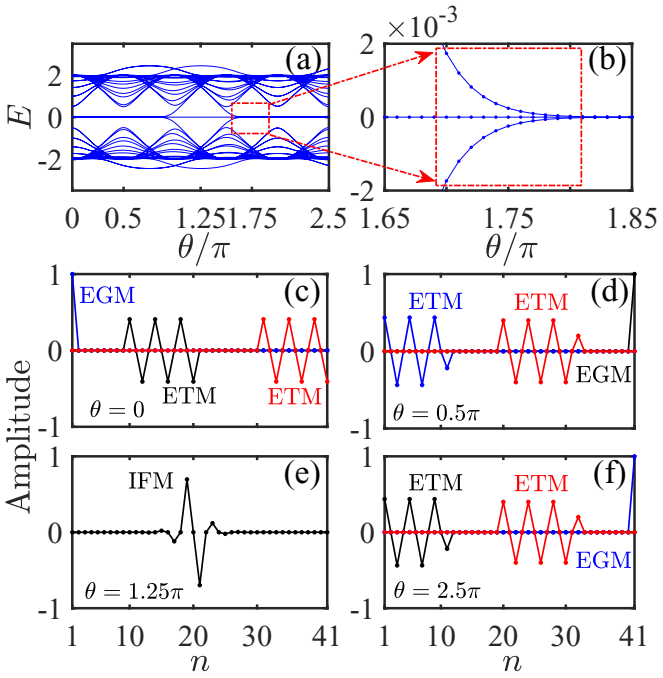

FIG. 2. Energy spectrum under the open boundary condition for an odd-sized splicing SSH chain. (a) Energy E vs the phase parameter θ. (b) Enlargement of the rectangular region in (a). (c)–(f) Zero-energy states corresponding to $\theta = 0, 0.5\pi, 1.25\pi$ and 2.5π, respectively. The other parameters are chosen to be $g_0 = g_1 = 1$, $N = 41$, and $(N_1, N_2, N_3, N_4) = (10, 10, 10, 11)$.

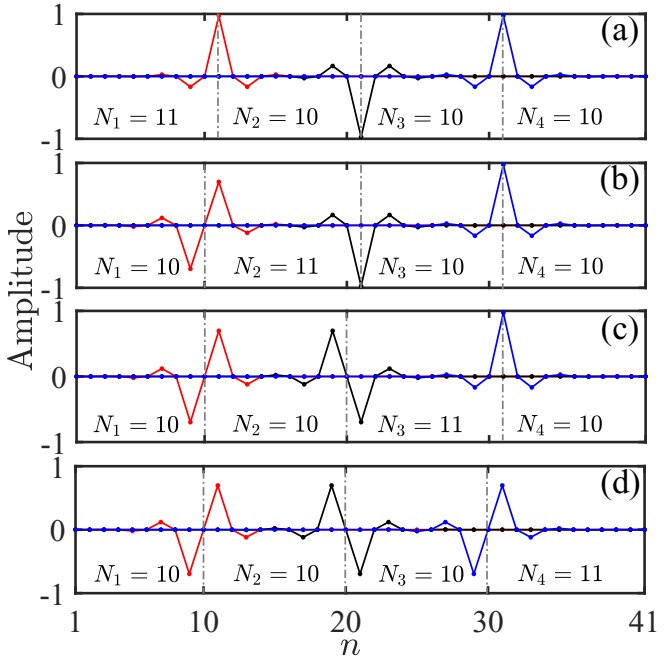

FIG. 3. The distribution of the zero-energy IFS. (a)–(d) The chain length of the splicing SSH chain is designed as $(N_1, N_2, N_2, N_4) = (11, 10, 10, 10)$, (10,11,10,10), (10,10,11,10), and (10,10,10,11), where the red, black, and blue zero-energy IFSs can be obtained at $\theta = 0.75$, 1.25, and 1.75, respectively. The other parameters are chosen to be $g_0 = g_1 = 1, N = 41$.

$\theta = 0, 0.5\pi, 1.25\pi$, and 2.5π in Figs. 2(c)–(f). It is shown that the zero-energy EGS and ETS can coexist for $\theta = 0, 0.5\pi$, and 2.5π, zero-energy IFSs can occur only for $\theta = 1.25\pi$, and the positions of zero-energy EGSs can be exchanged for $\theta = 0$ and 2.5π, which can provide an optimal QST protocol by adiabatically changing the parameter θ.

To study the influence of zero-energy IFSs on QST using the splicing-SSH-chain, we consider the distribution of zero-energy IFSs for different splicing forms to keep the total chain length ($N = 41$) unchanged in Fig. 3, where the gray dash-dotted lines correspond to the interface positions in the chain. Overall, we found that the distribution of zero-energy IFSs mainly includes two types; the first one is an even function of the splicing interface when the interface is at odd sites, and the second one is an odd function of the splicing interface when the interface is at even sites. The position of the occurring zero-energy IFS is at the first interface for $\theta = 0.75\pi$, the second interface for $\theta = 1.25\pi$, and the third interface for $\theta = 1.75\pi$.

Usually, in the process of QST for the case of a single-SSH-chain, in order to remain in the zero-energy eigenstate without exciting other eigenstates, one has to increase the transfer time T to ensure the adiabatic approximation. However, due to the decoherence of the quantum state under the evolution process, the large transfer time T will not only affect the feasibility of the experiment but also greatly reduce the transfer efficiency. Next, we will illustrate how to reach high-fidelity QST for small transfer time by using zero-energy IFS.

C. Speed of the transfer and phase diagram

Now let us examine in more detail the QST protocol that we described in the last section and provide numerical evidence supporting our claims. To do this, we consider the initial state of the system to be prepared in the zero-energy eigenstate, which is localized on the first site of the chain. In Figs. 4(a) and 4(b), we give the QST protocols for the splicing interface at even and odd sites by adiabatically changing the parameter θ from 0 to 2.5π in time T. We can see the QST from the leftmost end to the rightmost end of the chain can be perfectly realized regardless of whether the interface is at even sites or odd sites with the transfer time $T = 500$ and total chain length $N = 41$. To make a comparison in terms of the speed of the transfer, we plot the fidelity as a function of the transfer time for different protocols [see Fig. 4(c)]. Obviously, the transfer efficiency of splicing-SSH-chain protocols is much larger than that of the single-SSH-chain protocol. In addition, depending on the distribution of the zero-energy IFSs, the transfer efficiency of QST for the interface at even sites also is slightly better than that of the interface at odd sites when $T \leqslant 200$. The main reason is that the amplitude distribution of the zero-energy interface state involving the odd function, which is located on both sides of the splicing interface, is wider than the amplitude distribution of the even function, as shown in Fig. 3.

The QST depends not only on the transfer time T but also on the total length of the chain. We also consider the fidelity to vary with the total chain length N for a fixed transfer time (see Fig. 5). It is found that the advantage of the splicing-SSH-chain protocol is mainly reflected in the

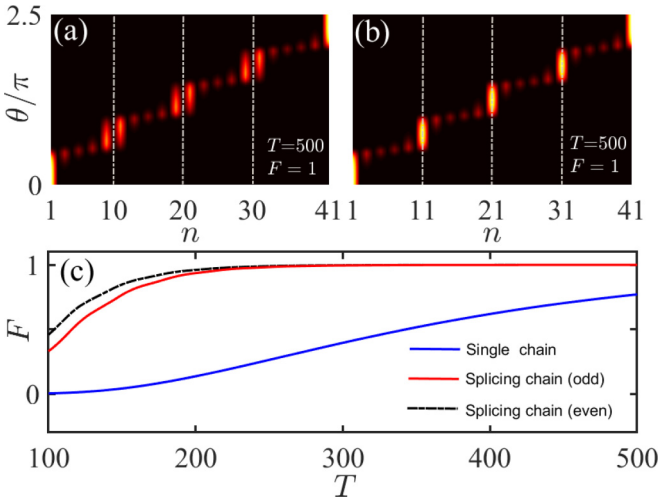

FIG. 4. (a) and (b) QST via splicing-SSH-chain protocols for the interface at even and odd sites. (c) The fidelity as a function of the transfer time for different protocols, where the black dashed line and red solid line correspond to the splicing-SSH-chain protocols of the interface at even and odd sites and the blue solid line corresponds to the single-SSH-chain protocol. The other parameters are chosen to be $g_0 = g_1 = 1, N = 41$.

long-distance QST because a nontrivial trade-off exists between the total chain length and the splicing path for a given value of transfer time (see the Appendix). If we define the fidelity $F > 0.99$, this means the quantum state is considered to be successfully transferred. For a fixed transfer time $T = 200$, the single-SSH-chain can successfully implement QST when total chain lengths are $N < 15$, while the splicing-SSH-chain cannot implement QST. However, the longest chain length of single SSH chain for successful QST is $N = 17$, while the

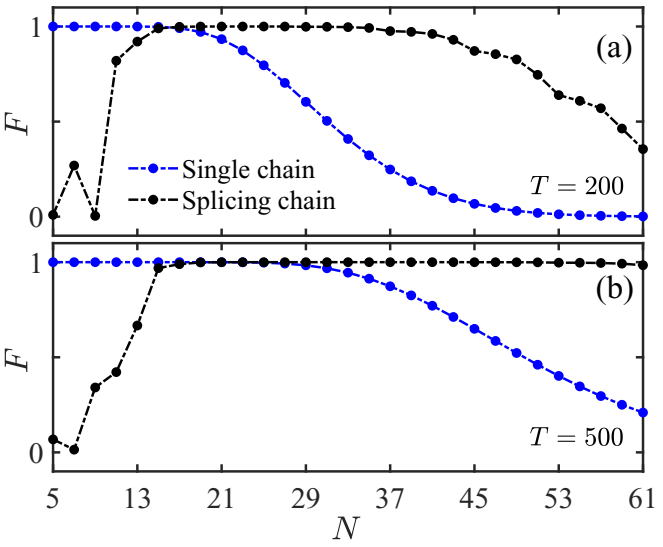

FIG. 5. The fidelity as a function of the total chain length N for a fixed transfer time (a) $T = 200$ and (b) $T = 500$, where blue and black dash-dotted lines correspond to the results of the single and splicing SSH chains, respectively. The other parameters are chosen to be $g_0 = g_1 = 1$.

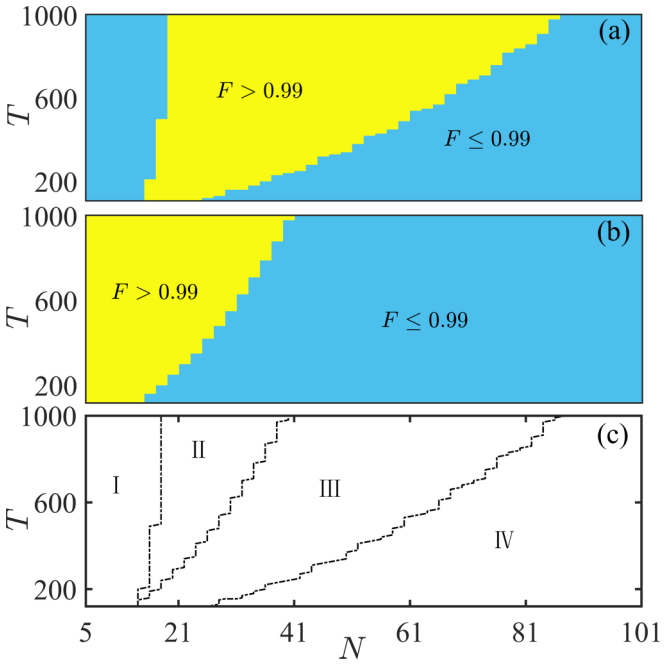

FIG. 6. Phase diagram of the quantum state transfer in the parameter space (T, N). (a) The result of the splicing SSH chain. (b) The result of the single SSH chain. (c) The total phase diagram derived from (a) and (b), where the parameter space can be divided into four regions. The other parameters are chosen to be $g_0 = g_1 = 1$.

longest chain length of splicing SSH chain is $N = 33$, which approaches double length compared with the case of single SSH chain [see Fig. 5(a)]. For comparison, we also consider the longer transfer time $T = 500$ in Fig. 5(b), where the longest chain length that can successfully implement QST is elongated. For the single-SSH-chain, the longest chain length for successful QST increases from $N = 17$ to 27, $\Delta N = 10$. For the splicing-SSH-chain, the longest chain length for successful QST increases from $N = 33$ to 55, $\Delta N = 22$. This means that for the splicing-SSH-chain, the total chain length that can successfully implement QST also increases faster along with the increase of transfer time T, compared to the case of single-SSH-chain. In addition, for a fixed total chain length and a given value of transfer time, one also can improve the efficiency of QST by using optimal splicing path (see the Appendix).

In contrast to previous single-SSH-chain protocols with the interchain couplings varied in time [3,10,44], our proposed scheme of the splicing-SSH-chain has greater advantages for experimental detection of QST. First, this scheme does not require a homogeneous chain. Second, this scheme also does not require the adiabatic change in the coupling strength to be uniform. Therefore, zero-energy IFSs in the splicing-SSH-chain may provide an experimentally friendly way to achieve QST. To this end, we show the phase diagram of the QST in parameter space (see Fig. 6). The yellow areas indicate that the QST can be successfully implemented, and the blue areas indicate the QST fails. Obviously, the parameter space can be divided into four regions according to different phase boundaries. In region I, the QST can be successfully implemented only via a single-SSH-chain. In region II, the QST can be

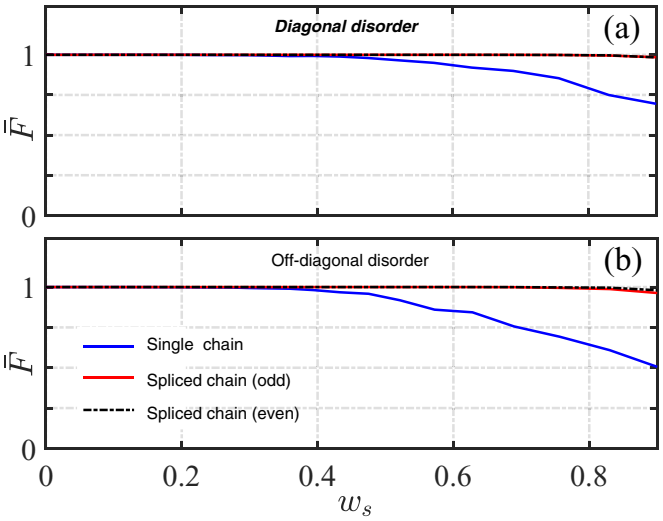

FIG. 7. The average fidelity as a function of the disorder strength w_s for different protocols and forms of disorder. The black dotted lines and red solid lines correspond to the results of the splicing SSH chain in which the splicing interfaces are at even and odd sites, and the blue solid lines are the results obtained via the single SSH chain. The other parameters are chosen to be $g_0 = g_1 = 1$, $N = 25$, and $T = 800$.

successfully implemented via a single- or splicing-SSH-chain. In region III, the QST can be successfully implemented only via the splicing-SSH-chain. In region IV, the QST cannot be implemented via a single- or splicing-SSH-chain. Therefore, depending on the different design schemes, we can choose the optimal QST protocol by adjusting only the phase parameter in the coupling. Our proposed protocol is experimentally more feasible than some previous protocols [3,43,44].

III. DISORDER ANALYSIS

Due to a manufacturing error that arises during experimental implementation, perfect modulation of the coupling strength is impossible. In this section, we now examine the robustness of the QST by introducing disorder both in the couplings and in the magnetic field and discuss its effect on fidelity. Generally, the disorder in the coupling is addressed as off-diagonal disorder, while the disorder in the magnetic field is addressed as diagonal disorder. The way each disorder realization is imposed on the system's parameters is as follows:

$$\begin{aligned} J_n &\to J_n(1+\delta J_n), \\ B_n &\to B_n + \delta B_n. \end{aligned} \tag{4}$$

Here, δJ_n and δB_n acquire random real values uniformly distributed in the interval $(-w_s, w_s)$, in which w_s corresponds to the disorder strength. When δJ_n and δB_n remain fixed during the time evolution, we call them static off-diagonal and diagonal disorder, respectively. For each sample we calculate fidelity F as a function of disorder strength w_s and then obtain the average fidelity $\bar{F}(w_s)$ by taking the average over all samples, $\bar{F}(w_s) = \frac{1}{M}\sum_{i=1}^{M} F$, where the total number of samples is $M = 200$ in our calculation.

In Fig. 7, for different protocols and forms of disorder, we plot the average fidelity as a function of w_s for total chain length $N = 25$. For the sake of comparison, we choose a set of parameters from region II in Fig. 6(c), where the QST can be successfully implemented via single or splicing SSH chains when $w_s = 0$. We can clearly see that, in the presence of the disorder (diagonal and off-diagonal) the protocols of splicing SSH chains have strong robustness, whose average fidelities always are $\bar{F} \to 1$ for $0 \leqslant w_s \leqslant 0.8$ regardless of whether disorder is diagonal or off-diagonal, while the average fidelity of the single-SSH-chain protocol is $\bar{F} \to 1$ for $0 \leqslant w_s \leqslant 0.4$, as shown in Figs. 7(a) and 7(b). In addition, the robustness against disorder of the splicing-SSH-chain protocol in which the interfaces are at odd or even sites is almost the same. To sum up, the splicing-SSH-chain protocol is quite robust to both diagonal and off-diagonal disorders and clearly outperforms the single-SSH-chain protocol.

IV. ENVIRONMENTAL EFFECT

For QST, environment-induced decoherence is an important issue. In the following, we consider the effect of environment on QST. For the environment, we consider that it mainly affects the first and last sites of the chain [45,46]. Then we add non-Hermitian on-site terms on the first and last sites,

$$\mathcal{H} = \sum_{n=1}^{N-1} J_n(|n\rangle\langle n+1| + \text{H.c.}) - i\gamma(|1\rangle\langle 1| - |N\rangle\langle N|), \tag{5}$$

where γ is the gain or loss parameter. If we now inject an initial wave function $\psi(0)$ into the chain, it will evolve as $\psi(T) = \psi(0)e^{-i\mathcal{H}(\theta)t}$ (we have set $\hbar = 1$). Due to the losses in the environment and the fact that all sites in the chain are coupled, we expect $|\psi(t)|^2$ to decrease over time. However, if the lossless zero-energy IFS also exists in the chain, for system sizes larger than the exponential confinement of the zero-energy edge state, the loss of a wave function injected at the edge state will be heavily suppressed. This loss suppression manifests in the propagator $e^{-i\mathcal{H}(\theta)t}$ through the existence of the imaginary components of the complex energies of the zero-energy IFS and EGS exponentially approaching zero with increasing system size.

This exact behavior of the energy of the system is observed in Fig. 8, which shows the real and imaginary energies as a function of the phase parameter θ. It is found that the imaginary components of the complex energies of the total system are complementary about $\theta = 1.25$; namely, the imaginary component is greater than zero for $\theta < 1.25$, while it is less than zero above $\theta > 1.25$ and vice versa. Crucially, the imaginary component of the zero-energy IFS is close to being purely real. This means that one can still implement QST assisted by zero-energy IFSs. In order to clarify the influence of the non-Hermitian term on QST, we give the fidelity as a function of the parameter γ in Fig. 9. We can see the splicing-SSH-chain protocol is also robust to the weak loss and clearly outperforms the single-SSH-chain protocol, and this robustness quickly increases with the system size, as shown in Figs. 9(a) and 9(b).

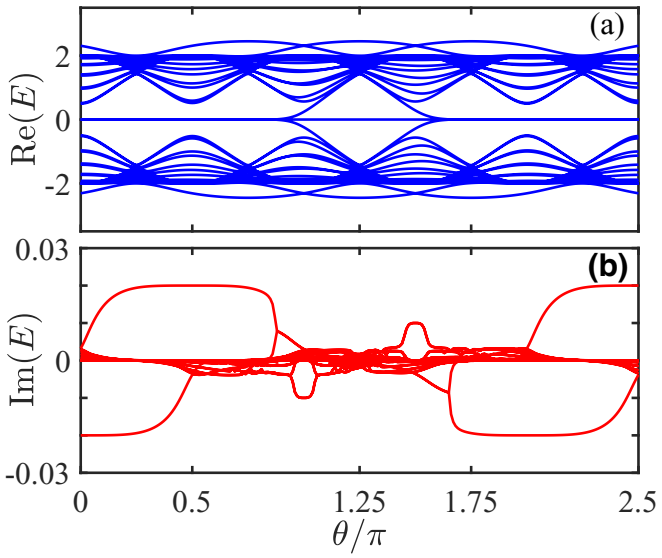

FIG. 8. Complex energies of the odd-sized splicing-SSH-chain as a function of the phase parameter θ. The other parameters are chosen to be $g_0 = g_1 = 1, N = 41, \gamma = 0.02$, and $(N_1, N_2, N_3, N_4) = (10, 10, 10, 11)$.

V. CONCLUSIONS

In this work we have investigated a fast, robust, and long-distance QST protocol that employs a splicing-SSH-chain to act as a quantum channel for transferring single-site excitations. We propose two types of zero-energy IFSs that can increase the efficiency of the transfer in terms of speed; the first one is an even function for the interfaces at odd sites, and the second one is an odd function for the interfaces at even sites. To sustain our claim, we made a comparison with the single-SSH-chain protocol. It was found that the existence of zero-energy IFSs not only can improve the speed of QST but also can realize long-distance QST. Furthermore, we gave the phase diagram in the parameter space of the transfer time T and the system size N. The different regions that can successfully implement QST were revealed via the single- or splicing-SSH-chain protocol. Therefore, we can choose the optimal QST protocol by adjusting only the coupling strength $J_{n,\varphi}$, where the single- or splicing-SSH-chain can be designed by adjusting the phase parameter φ. We studied the effect of diagonal and off-diagonal disorder on QST. It was revealed that the splicing-SSH-chain protocol is quite robust to both diagonal and off-diagonal disorders and clearly outperforms the single-SSH-chain protocol. We further considered the environmental influence by rendering the Hamiltonian non-Hermitian by allowing energy to radiate away; it was shown that the QST protocol assisted by zero-energy IFSs is more robust than previously expected and also outperforms the single-SSH-chain protocol. Our work may provide an experimentally friendly method for QST.

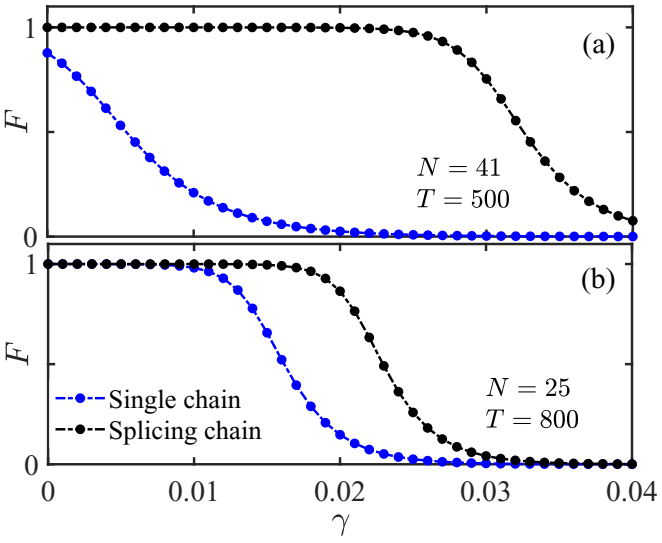

FIG. 9. The fidelity as a function of the parameter γ for a fixed total chain length and transfer time, (a) $N = 41, T = 500$ [region III in Fig. 6(c)] and (b) $N = 25, T = 800$ [region II in Fig. 6(c)], where blue and black dash-dotted lines correspond to the results of the single and splicing SSH chains, respectively. The other parameters are chosen to be $g_0 = g_1 = 1$.

ACKNOWLEDGMENTS

This work is supported by the National Natural Science Foundation of China under Grant No. 12175315, the Hunan Provincial Natural Science Foundation under Grants No. 2019JJ30044 and No. 2021JJ41062, the Scientific Research Fund of Hunan Provincial Education Department under Grant No. 19A510, and the Talent Project of Central South University of Forestry and Technology under Grant No. 2017YJ035.

APPENDIX: OPTIMAL SPLICING PATH FOR QUANTUM STATE TRANSFER

Because the coupling strength can periodically change $J_{n,\varphi} = J_{n,\varphi+2\pi}$, our system can be spliced by arbitrary numbers of SSH models by setting different coupling strengths $J_{n,\varphi}$. Of course, more splicing parts can lead to more interface states, which are conducive to quantum state transfer to a certain extent. However, for a given total chain length, when the numbers of splicing parts become big, the length of each splicing part will be shortened. There may exist an optimal splicing path for quantum state transfer for a fixed total chain length N and a given value of transfer time T. Through numerical calculation, we find that if the length of any splicing part is too short, $N_i < 4$, the quantum state transfer may be directly destroyed; the main reason is that the corresponding zero-energy interface state may be destroyed. In the following, we will show the nontrivial trade-off between the total chain length and the splicing path for a given value of transfer time via two examples.

To show the limit length of each splicing part, we first consider a short total chain length $N = 17$. As an example, for a fixed transfer time $T = 500$, we give the distribution of the zero-energy interface state and the corresponding quantum state transfer for three different splicing paths (see Fig. 10). We can see that if we choose the splicing path $(N_1, N_2, N_2, N_4) = (4, 4, 4, 5)$, the zero-energy interface states of the three interfaces that are an odd function of the splicing interface because the interfaces are at even sites can

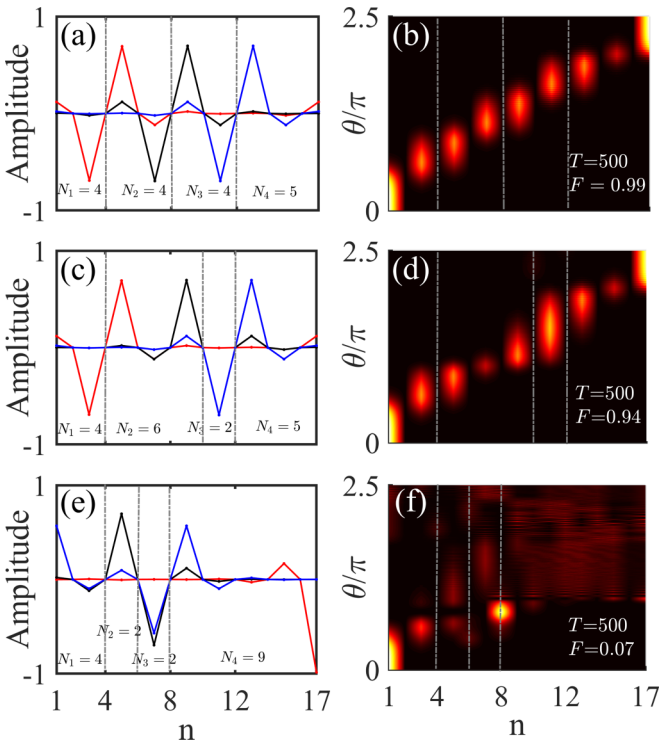

FIG. 10. The distribution of the zero-energy interface state and corresponding quantum state transfer for three different splicing paths with a fixed total chain length $N = 17$ and transfer time $T = 500$: (a) and (b) $(N_1, N_2, N_2, N_4) = (4, 4, 4, 5)$, (c) and (d) $(N_1, N_2, N_2, N_4) = (4, 6, 2, 5)$, and (e) and (f) $(N_1, N_2, N_2, N_4) = (4, 2, 2, 9)$.

be well preserved, and then the quantum state transfer can also be successfully implemented [see Figs. 10(a) and 10(b)]. If we choose the splicing path $(N_1, N_2, N_2, N_4) = (4, 6, 2, 5)$, the second zero-energy interface state causes deformation because the length of the third splicing part $N_3 = 2$ is less than four sites, and then the fidelity of the quantum state transfer also decreases to $F < 0.99$ [see Figs. 10(c) and 10(d)]. Especially, if we choose the splicing path $(N_1, N_2, N_2, N_4) = (4, 2, 2, 9)$, the first zero-energy interface state obviously is destroyed because the lengths of the second and third splicing parts $N_2 = 2$ and $N_3 = 2$ are less than four sites, which directly leads to the failure of quantum state transfer [see Figs. 10(e) and 10(f)]. To show the constructive effect of more

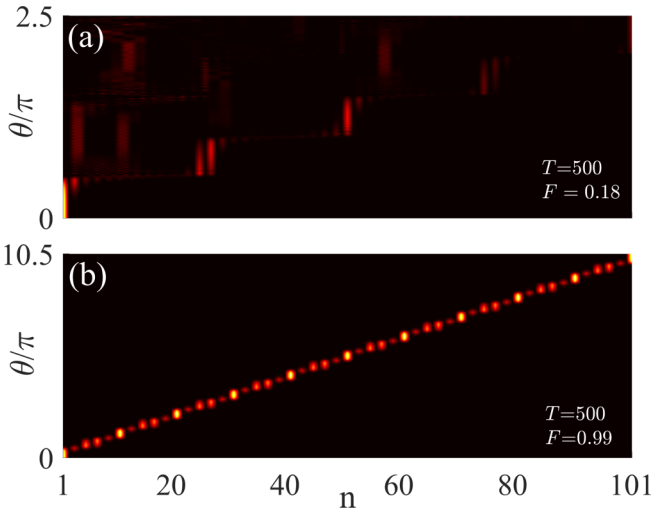

FIG. 11. The quantum state transfer for two different splicing paths with a fixed total chain length $N = 101$ and transfer time $T = 500$: (a) $(N_1, N_2, N_2, N_4) = (26, 25, 25, 25)$ and (b) $(N_1, N_2, N_2, N_4, \ldots, N_{20}) = (6, 5, 5, 5, \ldots, 5)$.

interface states on quantum state transfer, we consider a long total chain length $N = 101$. As an example, for a fixed transfer time $T = 500$, we give the quantum state transfer for two different splicing paths (see Fig. 11). We can see that if we choose the splicing path $(N_1, N_2, N_2, N_4) = (26, 25, 25, 25)$, although the system has four zero-energy interface states, quantum state transfer fails to occur because the transfer time is too short [see Fig. 11(a)]. If we choose the splicing path $(N_1, N_2, N_2, N_4, \ldots, N_{20}) = (6, 5, 5, 5, \ldots, 5)$, the quantum state transfer from the left end to the right end of the chain can be perfectly realized with the assistance of more interface states [see Fig. 11(b)]. Therefore, a nontrivial trade-off exists between the total chain length and the splicing path for a given value of transfer time; namely, the length of any splicing part is not less than four sites, $N_i \geqslant 4$. Under this splicing limit, more zero-energy interface states not only can improve the speed of quantum state transfer but also can realize long-distance quantum state transfer for a given transfer time. Without loss of generality, to show only the constructive effect of zero-energy interface states on quantum state transfer, we consider a periodic change in the coupling strength in our work; namely, our system is spliced by four parts.

[1] M. Christandl, N. Datta, A. Ekert, and A. J. Landahl, Perfect State Transfer in Quantum Spin Networks, Phys. Rev. Lett. **92**, 187902 (2004).

[2] L. Banchi, T. J. G. Apollaro, A. Cuccoli, R. Vaia, and P. Verrucchi, Long quantum channels for high-quality entanglement transfer, New J. Phys. **13**, 123006 (2011).

[3] S. Tan, R. W. Bomantara, and J. Gong, High-fidelity and long-distance entangled-state transfer with Floquet topological edge modes, Phys. Rev. A **102**, 022608 (2020).

[4] M. Bellec, G. M. Nikolopoulos, and S. Tzortzakis, Faithful communication Hamiltonian in photonic lattices, Opt. Lett. **37**, 4504 (2012).

[5] A. Perez-Leija, R. Keil, A. Kay, H. Moya-Cessa, S. Nolte, L. C. Kwek, B. M. Rodríguez-Lara, A. Szameit, and D. N. Christodoulides, Coherent quantum transport in photonic lattices, Phys. Rev. A **87**, 012309 (2013).

[6] R. J. Chapman, M. Santadrea, Z. Huang, G. Corrielli, A. Crespi, M.-H. Yung, R. Osellame, and A. Peruzzo, Experimental perfect state transfer of an entangled photonic qubi., Nat. Commun. **7**, 11339 (2016).

[7] Y. X. Shen, Y. G. Peng, D. G. Zhao, X. C. Chen, J. Zhu, and X. F. Zhu, One-Way Localized Adiabatic Passage in an Acoustic System, Phys. Rev. Lett. **122**, 094501 (2019).

[8] N. Y. Yao, L. Jiang, A. V. Gorshkov, Z. X. Gong, A. Zhai, L. M. Duan, and M. D. Lukin, Robust Quantum State Transfer in Random Unpolarized Spin Chains, Phys. Rev. Lett. **106**, 040505 (2011).

[9] D. I. Tsomokos, S. Ashhab, and F. Nori, Using superconducting qubit circuits to engineer exotic lattice systems, Phys. Rev. A **82**, 052311 (2010).

[10] F. Mei, G. Chen, L. Tian, S. L. Zhu, and S. T. Jia, Robust quantum state transfer via topological edge states in superconducting qubit chains, Phys. Rev. A **98**, 012331 (2018).

[11] D. Petrosyan and P. Lambropoulos, Coherent population transfer in a chain of tunnel coupled quantum dots, Opt. Commun. **264**, 419 (2006).

[12] Y. A. Chen, S. Nascimbène, M. Aidelsburger, M. Atala, S. Trotzky, and I. Bloch, Controlling Correlated Tunneling and Superexchange Interactions with ac-Driven Optical Lattices, Phys. Rev. Lett. **107**, 210405 (2011).

[13] P. Cappellaro, C. Ramanathan, and D. G. Cory, Simulations of Information Transport in Spin Chains, Phys. Rev. Lett. **99**, 250506 (2007).

[14] T. Tian, S. Lin, L. Zhang, P. Yin, P. Huang, C. Duan, L. Jiang, and J. Du, Perfect coherent transfer in an on-chip reconfigurable nanoelectromechanical network, Phys. Rev. B **101**, 174303 (2020).

[15] E. A. Sete, E. Mlinar, and A. N. Korotkov, Robust quantum state transfer using tunable couplers, Phys. Rev. B **91**, 144509 (2015).

[16] I. Brouzos, I. Kiorpelidis, F. K. Diakonos, and G. Theocharis, Fast, robust, and amplified transfer of topological edge modes on a time-varying mechanical chain, Phys. Rev. B **102**, 174312 (2020).

[17] M. H. Yung, Quantum speed limit for perfect state transfer in one dimension, Phys. Rev. A **74**, 030303(R) (2006).

[18] T. Caneva, M. Murphy, T. Calarco, R. Fazio, S. Montangero, V. Giovannetti, and G. E. Santoro, Optimal Control at the Quantum Speed Limit, Phys. Rev. Lett. **103**, 240501 (2009).

[19] M. Murphy, S. Montangero, V. Giovannetti, and T. Calarco, Communication at the quantum speed limit along a spin chain, Phys. Rev. A **82**, 022318 (2010).

[20] S. Ashhab, P. C. de Groot, and F. Nori, Speed limits for quantum gates in multiqubit systems, Phys. Rev. A **85**, 052327 (2012).

[21] S. Deffner and S. Campbell, Quantum speed limits: From Heisenberg's uncertainty principle to optimal quantum control, IOP Sci. **50**, 453001 (2017).

[22] J. M. Epstein and K. B. Whaley, Quantum speed limits for quantum-information-processing tasks, Phys. Rev. A **95**, 042314 (2017).

[23] X. M. Zhang, Z. W. Cui, X. Wang, and M. H. Yung, Automatic spin-chain learning to explore the quantum speed limit, Phys. Rev. A **97**, 052333 (2018).

[24] G. De Chiara, D. Rossini, S. Montangero, and R. Fazio, From perfect to fractal transmission in spin chains, Phys. Rev. A **72**, 012323 (2005).

[25] D. Burgarth and S. Bose, Conclusive and arbitrarily perfect quantum-state transfer using parallel spin-chain channels, Phys. Rev. A **71**, 052315 (2005).

[26] A. Kay, Perfect state transfer: Beyond nearest-neighbor couplings, Phys. Rev. A **73**, 032306 (2006).

[27] V. Balachandran and J. Gong, Adiabatic quantum transport in a spin chain with a moving potential, Phys. Rev. A **77**, 012303 (2008).

[28] J. Allcock and N. Linden, Quantum Communication beyond the Localization Length in Disordered Spin Chains, Phys. Rev. Lett. **102**, 110501 (2009).

[29] D. Petrosyan, G. M. Nikolopoulos, and P. Lambropoulos, State transfer in static and dynamic spin chains with disorder, Phys. Rev. A **81**, 042307 (2010).

[30] M. Bruderer, K. Franke, S. Ragg, W. Belzig, and D. Obreschkow, Exploiting boundary states of imperfect spin chains for high-fidelity state transfer, Phys. Rev. A **85**, 022312 (2012).

[31] R. R. Agundez, C. D. Hill, L. C. L. Hollenberg, S. Rogge, and M. Blaauboer, Superadiabatic quantum state transfer in spin chains, Phys. Rev. A **95**, 012317 (2017).

[32] B. H. Huang, Y. H. Kang, Y. H. Chen, Z. C. Shi, J. Song, and Y. Xia, Quantum state transfer in spin chains via shortcuts to adiabaticity, Phys. Rev. A **97**, 012333 (2018).

[33] A. Kiely and S. Campbell, Fast and robust magnon transport in a spin chain, New J. Phys. **23**, 033033 (2021).

[34] T. Fukuhara, A. Kantian, M. Endres, M. Cheneau, P. Schauß, S. Hild, D. Bellem, U. Schollwöck, T. Giamarchi, C. Gross, I. Bloch, and S. Kuhr, Quantum dynamics of a mobile spin impurity, Nat. Phys. **9**, 235 (2013).

[35] N. Y. Yao, C. R. Laumann, A. V. Gorshkov, H. Weimer, L. Jiang, J. I. Cirac, P. Zoller, and M. D. Lukin, Topologically protected quantum state transfer in a chiral spin liquid, Nat. Commun. **4**, 1 (2013).

[36] M. W. Doherty, N. B. Manson, P. Delaney, F. Jelezko, J. Wrachtrup, and L. C. L. Hollenberg, The nitrogen-vacancy colour centre in diamond, Phys. Rep. **528**, 1 (2013).

[37] D. D. Awschalom, L. C. Bassett, A. S. Dzurak, E. L. Hu, and J. R. Petta, Quantum spintronics: Engineering and manipulating atom-like spins in semiconductors, Science **339**, 1174 (2013).

[38] M. Metcalfe, Applications of cavity optomechanics, Appl. Phys. Rev. **1**, 031105 (2014).

[39] J. K. Asbóth, L. Oroszlány, and A. Pályi, in *A Short Course on Topological Insulators*, Lecture Notes in Physics Vol. 919 (Springer, Berlin, 2016), p. 166.

[40] C. Dlaska, B. Vermersch, and P. Zoller, Robust quantum state transfer via topologically protected edge channels in dipolar arrays, Quantum Sci. Technol. **2**, 015001 (2017).

[41] H. Bernien, S. Schwartz, A. Keesling, H. Levine, A. Omran, H. Pichler, S. Choi, A. S Zibrov, M. Endres, M. Greiner, V. Vuletic, and M. D. Lukin, Probing many-body dynamics on a 51-atom quantum simulator, Nature (London) **551**, 579 (2017).

[42] D. Obana, F. Liu, and K. Wakabayashi, Topological edge states in the Su-Schrieffer-Heeger model, Phys. Rev. B **100**, 075437 (2019).

[43] F. M. D'Angelis, F. A. Pinheiro, D. Guéry-Odelin, S. Longhi, and F. Impens, Fast and robust quantum state transfer

in a topological Su-Schrieffer-Heeger chain with next-to-nearest-neighbor interactions, Phys. Rev. Research **2**, 033475 (2020).

[44] N. E. Palaiodimopoulos, I. Brouzos, F. K. Diakonos, and G. Theocharis, Fast and robust quantum state transfer via a topological chain, Phys. Rev. A **103**, 052409 (2021).

[45] B. Zhu, R. Lü, and S. Chen, Pt symmetry in the non-Hermitian Su-Schrieffer-Heeger model with complex boundary potentials, Phys. Rev. A **89**, 062102 (2014).

[46] M. Klett, H. Cartarius, D. Dast, J. Main, and G. Wunner, Relation between $\mathcal{PT}$-symmetry breaking and topologically nontrivial phases in the Su-Schrieffer-Heeger and Kitaev models, Phys. Rev. A **95**, 053626 (2017).